

S1 Revised fragmentation table development

The revised CV-UMR-ToF-ACSM fragmentation table development is based on catalogued and newly collected CV-HR-ToF-AMS and CV-UMR-ToF-ACSM mass spectra. The CV-HR-ToF-AMS mass spectra are retrieved from the AMS spectral database (http://cires.lcolorado.edu/jimenez-group/AMSSd_CV, last access: 6 November 2024), where a variety of nitrate-containing and non-nitrate organic aerosol (OA) were measured (see Tables S1 and S2).

Table S1. Summary of CV-HR-ToF-AMS mass spectra (both V-mode and W-mode) from the AMS spectral database used to obtain correlations between Org fragment mass. The organic aerosol (OA) spectra originated from chamber experiments, ambient, and laboratory measurements from different studies. The vaporizer temperature (T_{CV}) is also specified.

| Type | ID | Description | Citation | T_{CV} ($^{\circ}\text{C}$) | Campaign/location/time |
|--|---|--|-------------------|---------------------------------|---|
| Chamber experiment | 001 | SOA from α -pinene + O_3 in dark chamber chemistry (pinene+ O_3) | Hu et al. (2018a) | 600 | CU chambers, CU campus (Boulder, CO, US) |
| | 002 | SOA from 100 ppb δ -carene + NO_3 (carene+ NO_3) | Hu et al. (2018a) | 600 | |
| | 003 | SOA from 100 ppb α -pinene + NO_3 + $(\text{NH}_4)_2\text{SO}_4$ seed (pinene+ NO_3 + SO_4) | Hu et al. (2018a) | 600 | |
| Ambient positive matrix factorization (PMF) factor | 001 | Cooking OA (COA) | Hu et al. (2017) | 525 | Boulder study, CU campus (Boulder, CO, US, April 2013) |
| | 002 | Hydrocarbon-like OA (HOA) | Hu et al. (2017) | 525 | |
| | 003 | Oxygenated OA (OOA) | Hu et al. (2017) | 525 | |
| | 008 | Isoprene epoxydiols-derived SOA (IEPOX-SOA) | Hu et al. (2018b) | 550 | SOAS campaign (Centreville, AL, US, June-July 2013) |
| | 012 | More-oxidized oxygenated OA (MO-OOA) | Hu et al. (2018b) | 600 | KORUS-AQ study (RF05) flight (Seoul, South Korea, May 2016) |
| | 013 | Less-oxidized oxygenated OA (LO-OOA) | Hu et al. (2018b) | 600 | |
| | 014 | Hydrocarbon-like OA (HOA) | Hu et al. (2018b) | 600 | |
| Laboratory OA/SOA | 001 | Acetyl salicylic acid (AcSal-H, $\text{C}_9\text{H}_8\text{O}_4$) | Hu et al. (2018b) | 600 | CU laboratory, CU campus (Boulder, CO, US) |
| | 002 | Folic acid (folic-H, $\text{C}_{19}\text{H}_{19}\text{N}_7\text{O}_6$) | Hu et al. (2018b) | 600 | |
| | 006 | Caffeine ($\text{C}_8\text{H}_{10}\text{N}_4\text{O}_2$) | Hu et al. (2018b) | 600 | |
| | 007 | Histidine (His, $\text{C}_6\text{H}_9\text{N}_3\text{O}_2$) | Hu et al. (2018b) | 600 | |
| | 008 | Tryptophan (Try, $\text{C}_{11}\text{H}_{12}\text{N}_2\text{O}_2$) | Hu et al. (2018b) | 600 | |
| | 010 | Nicotinic acid (nicotinic-H, $\text{C}_6\text{H}_5\text{NO}_2$) | Hu et al. (2018b) | 600 | |
| | 011 | Sucrose (sucrose_1, $\text{C}_{12}\text{H}_{22}\text{O}_{11}$) | Hu et al. (2018b) | 600 | |
| | 015 | Oleic acid (oleic-H_1, $\text{C}_{18}\text{H}_{34}\text{O}_2$) | Hu et al. (2018b) | 600 | |
| | 016 | Squalene (squalene_1, $\text{C}_{30}\text{H}_{50}$) | Hu et al. (2018b) | 600 | |
| | 018 | Bis-(2-ethylhexyl)-ester (bis(2-EtHex)ester, $\text{C}_{26}\text{H}_{50}\text{O}_4$) | Hu et al. (2018a) | 600 | |
| | 020 | Oleic acid (oleic-H_2, $\text{C}_{18}\text{H}_{34}\text{O}_2$) | Hu et al. (2018a) | 600 | |
| | 021 | Squalene (squalene_2, $\text{C}_{30}\text{H}_{50}$) | Hu et al. (2018a) | 600 | |
| | 023 | Glutaric acid (glutaric-H, $\text{C}_5\text{H}_8\text{O}_4$) | Hu et al. (2018a) | 600 | |
| 024 | Octacosane ($\text{C}_{28}\text{H}_{58}$) | Hu et al. (2018a) | 550 | | |
| 026 | Sucrose (sucrose_2, $\text{C}_{12}\text{H}_{22}\text{O}_{11}$) | Hu et al. (2018a) | 600 | | |

The chamber experiment spectra were obtained from CU Atmospheric Chamber facility (Boulder, Colorado, United States, see Hu et al. (2018a)). The ambient PMF factors were measured at different locations: three spectra at the University of Colorado during spring (Boulder, Colorado, United States, (Hu et al., 2017)), one spectrum from SOAS campaign at a pollution-influenced forest site during summer (Centreville, Alabama, United States, (Carlton et al., 2018; Hu et al., 2018b)), and three spectra from an aircraft-based field campaign as part of KOREan-United States Air Quality mission (KORUS-AQ, <https://espo.nasa.gov/home/korus-aq>, last access: 6 November 2024). The laboratory standard measurements account for 15

mass spectra, ranging from carboxylic acids, hydrocarbons, nitrogen-containing compounds, and amino acids. Table S1 lists all of the OA datasets used, including both experiments containing and not containing nitrate.

15 The CV-UMR-ToF-ACSM mass spectra measured in chamber experiments when there is no or negligible nitrate present are summarized in Table S2. Because these are UMR spectra, we cannot use any experiments that contained nitrate. Therefore, the investigated nominal masses are assumed to contain only Org fragments (m/z 29, m/z 30, m/z 42, m/z 43, m/z 45, m/z 46). The chamber experiments were conducted in Aerosol Interaction and Dynamics in the Atmosphere (AIDA) chamber, a facility maintained by Institute of Meteorology and Climate Research (IMK) in Karlsruhe Institute of Technology (KIT), Germany. The experiments were part of the Cloud-Aerosol Interactions in a Nitrogen-dominated Atmosphere (CAINA) project
20 (<https://sites.google.com/view/cainaproject/>, last access: 6 November 2024).

Table S2. Summary of CV-UMR-ToF-ACSM mass spectra from nitrate-free chamber experiments used to obtain correlations between Org fragment mass. The mass spectra are measured using ACSM-RUG with vaporizer temperature (T_{CV}) of 525 °C.

| Type | ID | Description | Campaign/location/time |
|--------------------|-----|--|---------------------------------------|
| Chamber experiment | 004 | SOA from isoprene + O ₃ + TME + (NH ₄) ₂ SO ₄ seed in dark chamber (isoprene+O ₃ +TME(+AmS)) | AIDA chamber, IMK KIT (Karlsruhe, DE) |
| | 005 | SOA from α -pinene + O ₃ + TME + NaCl seed in dark chamber (pinene+O ₃ +TME(+NaCl)) | |
| | 006 | SOA from glyoxal + (NH ₄) ₂ SO ₄ seed in dark chamber (glyoxal(+AmS)_1) | |
| | 007 | SOA from glyoxal + NaCl seed in dark chamber (glyoxal(+NaCl)_1) | |
| | 008 | SOA from glyoxal + (NH ₄) ₂ SO ₄ seed in dark chamber (glyoxal(+AmS)_2) | |
| | 009 | SOA from glyoxal + NaCl seed in dark chamber (glyoxal(+NaCl)_2) | |

The slope of the orthogonal distance regression (ODR) fits to determine the multiplier $a_{\text{Org}[30],[i]}$ and $a_{\text{Org}[46],[i]}$ using the simulated UMR spectra (of the HR dataset) and UMR dataset are summarized in Table S3. The uncertainty of the value from the fit slope is also included. To confirm the best fit of the multipliers, the predicted UMR mass (calculated using the multiplier) is compared to the measured UMR mass (sum of mass measured in original spectra) which is resumed in Table S4.

Table S3. Summary of the ODR fit parameters with intercept at zero between different UMR nominal mass to predict (frag_Org[x]) and related UMR nominal mass (frag_Org[i]) from the full dataset (frag_Org[x] = $a_{\text{Org}[x],[i]}$ · frag_Org[i]). The slope is defined as the multiplier $a_{\text{Org}[x],[i]}$ which defines the fractional relation between the two UMR masses investigated.

| UMR mass to predict (x) | frag_Org[30] = $a_{\text{Org}[30],[i]}$ · frag_Org[i] | | | frag_Org[46] = $a_{\text{Org}[46],[i]}$ · frag_Org[i] | | |
|-----------------------------|---|-------------|----------|---|-------------|----------|
| UMR daughter mass (i) | $a_{\text{Org}[\text{CH}_2\text{O}^+],[i]} \pm s_a$ | r^2 | χ^2 | $a_{\text{Org}[\text{CH}_4\text{NO}^+],[i]} \pm s_a$ | r^2 | χ^2 |
| frag_Org[29] | 0.311 ± 0.016 | 0.88 | 1.57E-3 | (3.17 ± 2.49)E-3 | 0.11 | 4.27E-5 |
| frag_Org[42] | 0.963 ± 0.230 | 0.05 | 0.01 | 0.024 ± 0.006 | 0.01 | 3.06E-5 |
| frag_Org[43] | 0.367 ± 0.108 | 0.01 | 0.02 | 0.012 ± 0.004 | 1.70E-3 | 3.54E-5 |
| frag_Org[45] | 14.002 ± 3.559 | 0.02 | 2.33E-4 | 0.305 ± 0.037 | 0.43 | 1.35E-5 |

i represent masses related to frag_Org[30] (i.e., C¹⁸O⁺, ¹³CHO⁺, CH₂O⁺, CH₄N⁺, ¹³CH₃N⁺, ¹³CCH₅⁺, C₂H₆⁺) and frag_Org[46] (i.e., C¹⁸OO⁺, ¹³CHO₂⁺, CH₂O₂⁺, ¹³CH₃NO⁺, CH₄NO⁺, ¹³CCH₅O⁺, C₂H₆O⁺) tested in this study. It includes frag_Org[29] (i.e., ¹³CO⁺, CHO⁺, CH₃N⁺, C₂H₅⁺), frag_Org[42] (i.e., ¹³CCHO⁺, C₂H₂O⁺, C₂H₄N⁺, C₂H₃¹⁵N⁺, ¹³CCH₃N⁺, C₂H₄⁺, ¹³CC₂H₅⁺, C₃H₆⁺), frag_Org[43] (i.e., CHNO⁺, ¹³CCH₂O⁺, C₂H₃O⁺, C₂H₄¹⁵N⁺, ¹³CCH₄N⁺, C₂H₅N⁺, ¹³CC₂H₆⁺, C₃H₇⁺), and frag_Org[45] (i.e., ¹³CO₂⁺, CHO₂⁺, ¹³CH₂NO⁺, CH₃NO⁺, ¹³CCH₄O⁺, C₂H₅O⁺, ¹³CCH₆N⁺, C₂H₇N⁺, ¹³C₂CH₇⁺, ¹³CC₂H₈⁺). The choice is based on the list studied in Fry et al. (2018).

$a_{\text{Org}[x],[i]}$ is the coefficient for frag_Org[x] component, obtained from the slope of linear regression fit between frag_Org[x] and frag_Org[i]. Values printed in **bold** represent the best correlation for frag_Org[x].

Table S4. The multipliers $a_{\text{Org}[x],[i]} \cdot \text{frag_Org}[i]$ for $\text{frag_Org}[30]$ and $\text{frag_Org}[46]$ from this study and other studies, re-applied to the simulated UMR spectra from the HR and UMR datasets.

| Work | $a_{\text{Org}[30],[29]}$ | Predicted/ measured ^(a) $\text{frag_Org}[30] = a_{\text{Org}[30],[29]} \cdot \text{frag_Org}[29]$ | r^2 | χ^2 | $a_{\text{Org}[46],[45]}$ | Predicted/ measured ^(a) $\text{frag_Org}[46] = a_{\text{Org}[46],[45]} \cdot \text{frag_Org}[45]$ | r^2 | χ^2 |
|--|---------------------------|--|-------|----------|---------------------------|--|-------|----------|
| this study (CV-ToF)^(b) | 0.311±0.016 | (96.9±4.9)% | 0.88 | 8.48E-4 | 0.305±0.037 | (82.5±9.5)% | 0.43 | 6.79E-6 |
| Allan et al. (2004) (default) | 0.022 | (6.6±3.4)% | 0.88 | 8.03E-6 | - | - | - | - |
| Fry et al. (2018) (SV-ToF) | 0.215 | (66.0±3.3)% | 0.88 | 5.40E-4 | 0.127 | (30.3±3.7)% | 0.43 | 1.71E-6 |
| Hu et al. (2017) (biogenic, SV-ToF) | 0.31 | (96.4±4.8)% | 0.88 | 8.44E-4 | 0.42 | (121.7±14.0)% | 0.43 | 9.34E-6 |
| Hu et al. (2017) (biogenic, CV-ToF) | 0.31 | (99.7±5.0)% | 0.88 | 8.71E-4 | 0.68 | (214.4±25.5)% | 0.43 | 1.22E-5 |

^(a) data from CV-ToF-AMS spectral database and experiments in AIDA chamber described in Table S1 and S2, fit for typical ambient dataset. Values printed in **bold** represent the best correlation for $\text{frag_Org}[x]$.

^(b) predicted UMR $\text{frag_Org}[x]$ (calculated from dataset spectra, $\text{frag_Org}[x] = a_{\text{Org}[x],[i]} \cdot \text{frag_Org}[i]$) vs measured $\text{frag_Org}[x]$ (sum of all Org fragments in the nominal m/z x of the original dataset spectra).

25 We also explore different multipliers that are compatible for different composition profile. We perform the ODR fit of $\text{frag_Org}[30]$ against $\text{frag_Org}[29]$, and $\text{frag_Org}[46]$ against $\text{frag_Org}[45]$ to chamber experiment spectra that use glyoxal and terpenes (e.g., isoprene, limonene) as precursor to obtain composition-specific fragmentation table for each (see Fig. S1).

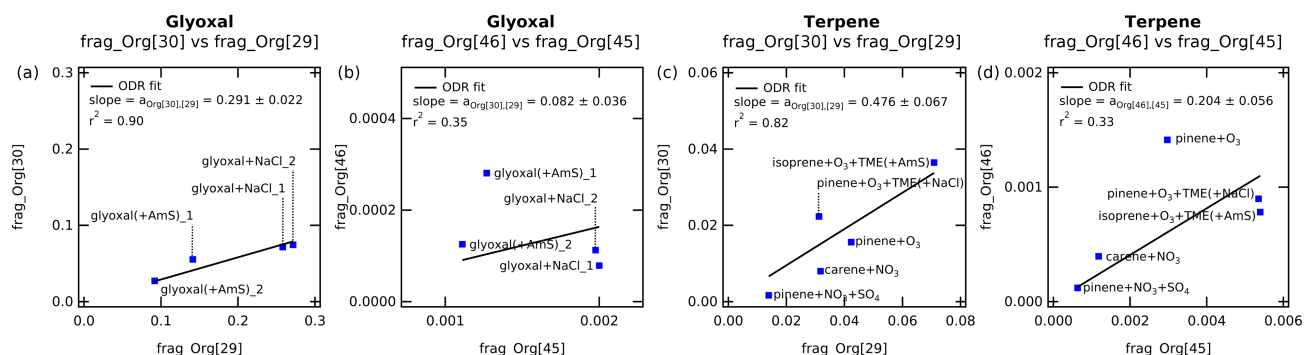


Figure S1. The ODR fits (set to zero intercept) to determine the multipliers $a_{\text{Org}[x],[i]}$ for composition-specific fragmentation table of (a,b) glyoxal and (c,d) terpene. The ODR fits show the correlation between the concentrations of (a,c) $\text{frag_Org}[30]$ vs $\text{frag_Org}[29]$, and (b,d) $\text{frag_Org}[46]$ vs $\text{frag_Org}[45]$.

30 Higher uncertainty shows more variability of organic fragment composition that leads to uncertainties for $\text{frag_NO}_3[30]$ and $\text{frag_NO}_3[46]$, which later affect the calculation of observed NO_3^+ ratio (R_{obs}) and mass fraction of NO_3 existing as particulate organic nitrate (f_{PON}).

S2 Summary of experimental R_{pAmN} of CV-UMR-ToF-ACSM

The measurements of R_{pAmN} from two CV-UMR-ToF-ACSM instruments used in the main article are summarized in Table S5.

Table S5. Summary of measured NO_x^+ ratio of particulate ammonium nitrate (R_{pAmN}) from two CV-UMR-ToF-ACSM in the Netherlands, as part of routine calibration measurements. The uncertainty on each measurement is included. The value is obtained by performing ODR fits to zero intercept of the concentration of m/z 46 against m/z 30 (no fragmentation table applied). The instruments are part of the Ruisdael Observatory monitoring site network in the Netherlands managed by different institutions: ACSM-UU by Utrecht University (UU) and ACSM-RUG by University of Groningen (RUG).

| Location | Date (dd/mm/yyyy) | $R_{amb} \pm s_R$ | r^2 | χ^2 |
|--|----------------------|---------------------------------------|-------|----------|
| ACSM UU | | | | |
| CESAR tower, Cabauw, Netherlands | 09/04/2021 | 0.0227 ± 0.0005 | 0.94 | 7.54E-4 |
| CESAR tower, Cabauw, Netherlands | 16/04/2021 | 0.0233 ± 0.0005 | 0.98 | 9.47E-4 |
| CESAR tower, Cabauw, Netherlands | 27/07/2021 | 0.0253 ± 0.0003 | 0.99 | 2.47E-3 |
| CESAR tower, Cabauw, Netherlands | 14/04/2023 | 0.0232 ± 0.0002 | 0.99 | 3.56E-2 |
| LSCE CEA Paris-Saclay, France | 14/11/2023 | 0.0241 ± 0.0001 | 0.99 | 5.27E-2 |
| | Mean | 0.0237 ± 0.0009 | | |
| ACSM RUG | | | | |
| Lutjewad, Groningen, Netherlands | 08/03/2023 | 0.0114 ± 0.0002 | 0.98 | 3.75E-3 |
| LSCE CEA Paris-Saclay, France | 16/11/2023 | 0.0116 ± 0.0002 | 0.99 | 3.17E-3 |
| AIDA chamber IMK KIT, Karlsruhe, Germany | 09/01/2024 | 0.0112 ± 0.0001 | 0.99 | 1.88E-3 |
| | Mean | 0.0114 ± 0.0002 | | |

S3 "Excess NH_4 " method to determine lower limit of R_{pON} from chamber experiment

35 The values of NO_x^+ ratio of particulate organic nitrate (R_{pON}) in this study are determined from an AIDA chamber experiment at IMK KIT, Karlsruhe, Germany. The experiment, described in Section 4.2 of the main text, used glyoxal as an SOA precursor, reacted with NO_3 (from NO_2 and O_3), and used NaCl seed. The average NO_x^+ ratio observed during particulate organic nitrate (pON) formation is taken as R_{pON} if we assume all nitrate aerosol formed is pON from the reaction of NO_3 with glyoxal.

40 However, chamber experiments can contain impurities, for example, inorganic nitrate can also be formed from HNO_3 uptake or repartitioning of semi-volatile NH_4NO_3 from the chamber walls during pON formation. Therefore, it may not produce pure pON and the NO_x^+ ratio observed cannot necessarily be assumed to be R_{pON} . By removing the inorganic nitrate impurities through "excess NH_4 " method (Takeuchi and Ng, 2019), we define R_{pON} as the lower limit of R_{pON} because it represents the lowest possible NO_x^+ ratio.

45 The "excess NH_4 " method is a way to estimate the inorganic nitrate contribution to the total NO_3 based on the increase in NH_4 . It assumes that any increase in NH_4 during aerosol growth is entirely due to NH_4NO_3 formation (molar concentration of excess NH_4 = molar concentration of inorganic nitrate). From there, we can subtract this maximum inorganic nitrate mass from the total NO_3 to determine f_{pON} . By having information on f_{pON} , NO_x^+ ratio of particulate ammonium nitrate (R_{pAmN}), and observed NO_x^+ ratio (R_{obs}), we are able to determine the value of R_{pON} of any purity level of pON formation by rearranging Eq. S1 (Farmer et al., 2010) into Eq. S2.

$$f_{pON} = \frac{(R_{amb} - R_{pAmN})(1 + R_{pON})}{(R_{pON} - R_{pAmN})(1 + R_{amb})} \quad (S1)$$

$$50 \quad R_{pON} = \frac{(R_{obs} \cdot R_{pAmN} \cdot f_{pON}) + R_{obs} + (R_{pAmN} \cdot f_{pON}) - R_{pAmN}}{(R_{obs} \cdot f_{pON}) - R_{obs} + R_{pAmN} + f_{pON}} \quad (S2)$$

We consider this to be the highest estimate of the potential inorganic nitrate interference, because all NH_4 is not necessarily NH_4NO_3 . For example, there can be NH_4Cl formed since in this experiment we have NaCl seed aerosol.

S4 Propagation of uncertainty

55 The value of f_{pON} is calculated from measurements that contain uncertainties as part of its measurement (see Eq. S1). In this section, we describe in detail how the uncertainty is propagated from different measurements acquired using the UMR instrument and fragmentation table, or HR instrument and peak fitting, into f_{pON} . Overall, the uncertainties for f_{pON} are sourced from 3 main parameters, which are the NO_x^+ ratio of the observed air (R_{obs}), pure ammonium nitrate (R_{pAmN}), and pure organic nitrate (R_{pON}). Each ratio itself is calculated from values containing uncertainties. In this work, the uncertainty is propagated from the standard error ($s_{\bar{x}}$) of the sample (Eq. S3).

$$60 \quad s_{\bar{x}} = \frac{s}{\sqrt{N}} = \frac{1}{\sqrt{N}} \cdot \sqrt{\frac{1}{N-1} \sum_{i=1}^N (x_i - \bar{x})^2} \quad (\text{S3})$$

x_i : data point i of variable x

\bar{x} : mean of data points

N : number of data points.

S4.1 R_{obs}

65 For UMR measurements, R_{obs} is calculated using observed ion concentrations (C_{NO^+} and $C_{\text{NO}_2^+}$) measured while sampling ambient or chamber generated particles, as described in the revised fragmentation table (see Table 4), rewritten in Eq. S4 below,

$$R_{\text{obs}} = \frac{(C_{\text{NO}_2^+})_{\text{obs}}}{(C_{\text{NO}^+})_{\text{obs}}} = \frac{C_{[46]} - a_{\text{Org}[46],[45]} \cdot C_{[45]}}{C_{[30]} - a_{\text{Org}[30],[29]} \cdot C_{[29]}}. \quad (\text{S4})$$

Therefore, R_{obs} contains in total of six uncertainty terms. Four uncertainty sources originated from the measured concentrations of m/z x ($C_{[x]}$, $x = [29,30,45,46]$). The uncertainty is generated by Tofware v3.3, which is described as being calculated based on ion counting statistics and an estimated electronic noise of the instrument.

70 The other two uncertainties come from the multipliers $a_{\text{Org}[30],[29]}$ and $a_{\text{Org}[46],[45]}$ represented by the uncertainty of ODR fits described in Table S3. While the uncertainty from concentrations varies over the course of time, the uncertainty from the multipliers remains constant. The propagated uncertainty of R_{obs} ($s_{\bar{R}_{\text{obs}}}$), see Eq. S7) is calculated from the uncertainty of NO_2^+ concentration ($s_{\bar{C}_{\text{NO}_2^+}}$), see Eq. S5) and NO^+ concentration ($s_{\bar{C}_{\text{NO}^+}}$), see Eq. S6),

$$75 \quad s_{\bar{C}_{\text{NO}_2^+}} = \sqrt{(s_{\bar{C}_{[46]}})^2 + \left(a_{\text{Org}[46],[45]} \cdot C_{[45]} \cdot \sqrt{\left(\frac{s_{\bar{a}_{\text{Org}[46],[45]}}}{a_{\text{Org}[46],[45]}} \right)^2 + \left(\frac{s_{\bar{C}_{[45]}}}{C_{[45]}} \right)^2} \right)^2} \quad (\text{S5})$$

$$s_{\bar{C}_{\text{NO}^+}} = \sqrt{(s_{\bar{C}_{[30]}})^2 + \left(a_{\text{Org}[30],[29]} \cdot C_{[29]} \cdot \sqrt{\left(\frac{s_{\bar{a}_{\text{Org}[30],[29]}}}{a_{\text{Org}[30],[29]}} \right)^2 + \left(\frac{s_{\bar{C}_{[29]}}}{C_{[29]}} \right)^2} \right)^2} \quad (\text{S6})$$

$$s_{\bar{R}_{\text{obs}}} = R_{\text{obs}} \cdot \sqrt{\left(\frac{s_{\bar{C}_{\text{NO}^+}}}{C_{\text{NO}^+}} \right)^2 + \left(\frac{s_{\bar{C}_{\text{NO}_2^+}}}{C_{\text{NO}_2^+}} \right)^2}. \quad (\text{S7})$$

For HR measurements, the NO^+ and NO_2^+ concentrations are obtained through HR peak fitting using PIKA module of ToF-AMS HR Analysis 1.26E. Therefore, $s_{(\bar{C}_{\text{NO}^+})_{\text{amb}}}$ and $s_{(\bar{C}_{\text{NO}_2^+})_{\text{amb}}}$ is simply the peak fitting uncertainty output by PIKA.

80 S4.2 R_{pAmN} and R_{pON}

As it is typical to measure particulate ammonium nitrate (pAmN) as part of the AMS/ACSM instrument calibration, we propagate the uncertainty of R_{pAmN} from repeated NH_4NO_3 calibration ($s_{\overline{R}_{\text{pAmN}}}$, see Eq. S8). It thus represents how much the instrument's response to pAmN diverges over the course of time. Therefore, R_{pAmN} contributes in total to one uncertainty term and is constant for each time point.

$$85 \quad s_{\overline{R}_{\text{pAmN}}} = \frac{1}{\sqrt{N}} \cdot \sqrt{\frac{1}{N-1} \sum_{i=1}^N (R_{\text{pAmN}_i} - \overline{R}_{\text{pAmN}})^2} \quad (\text{S8})$$

R_{pAmN_i} : calculated R_{pAmN} value from measurement i

$\overline{R}_{\text{pAmN}}$: average R_{pAmN} value

N : number of repeated pAmN measurements.

In this study, we omit the uncertainty of R_{pON} ($s_{\overline{R}_{\text{pON}}}$) from the propagation. Instead, the uncertainty of R_{pON} is obtained through the calculation of f_{pON} using the lower and upper limit of R_{pON} described in Section 4.2. By combining the propagation of uncertainty and the range of R_{pON} , the final uncertainty will include R_{obs} , R_{pAmN} , and R_{pON} .

S4.3 Propagation of uncertainty to the final function

The uncertainty is propagated as standard error from each variable, calculated using a simplified approach described in Eqs. S9 and S10. This approach is used because R_{obs} and R_{pAmN} appear several times in Eq. S1 to calculate f_{pON} . If we use the standard rule of uncertainty propagation, it will result in multiple representations of the same uncertainty in the calculation, which will lead to a higher propagated uncertainty. Simplified uncertainty propagation assumes independent, uncorrelated variables to yield a common function formula. The propagated uncertainty in the form of standard error of the function (s_f) is derived from the standard error (s_{x_i}) and the partially derived function ($\frac{\partial f}{\partial x_i}$) for each variable or uncertainty source, as defined by Eq. S9. The formula is applied to f_{pON} and gives the final uncertainty propagation equation as shown in Eq. S10, S11, S12, and S13.

$$100 \quad s_{f(x_i, x_{i+1}, \dots)} = \sqrt{\sum_{i=1}^N \left(\frac{\partial f(x_i, x_{i+1}, \dots)}{\partial x_i} \right)^2 \cdot s_{x_i}^2} \quad (\text{S9})$$

$$s_{f_{\text{pON}}} = \sqrt{\left(\frac{\partial f_{\text{pON}}}{\partial R_{\text{obs}}} \right)^2 \cdot s_{R_{\text{obs}}}^2 + \left(\frac{\partial f_{\text{pON}}}{\partial R_{\text{pAmN}}} \right)^2 \cdot s_{R_{\text{pAmN}}}^2 + \left(\frac{\partial f_{\text{pON}}}{\partial R_{\text{pON}}} \right)^2 \cdot s_{R_{\text{pON}}}^2} \quad (\text{S10})$$

By taking f_{pON} from Eq. S1, the partial derivatives are as follows:

$$\frac{\partial f_{\text{pON}}}{\partial R_{\text{obs}}} = \frac{(R_{\text{pAmN}} + 1) \cdot (R_{\text{pON}} + 1)}{(R_{\text{obs}} + 1)^2 \cdot (R_{\text{pON}} - R_{\text{pAmN}})} \quad (\text{S11})$$

$$\frac{\partial f_{\text{pON}}}{\partial R_{\text{pAmN}}} = \frac{(R_{\text{obs}} - R_{\text{pON}}) \cdot (R_{\text{pON}} + 1)}{(R_{\text{obs}} + 1) \cdot (R_{\text{pON}} - R_{\text{pAmN}})^2} \quad (\text{S12})$$

$$105 \quad \frac{\partial f_{\text{pON}}}{\partial R_{\text{pON}}} = \frac{(-R_{\text{pAmN}} - 1) \cdot (R_{\text{obs}} - R_{\text{pAmN}})}{(R_{\text{obs}} + 1) \cdot (R_{\text{pON}} - R_{\text{pAmN}})^2} \quad (\text{S13})$$

To propagate the uncertainty further into concentration, we combine the final uncertainty of f_{pON} and the total concentration of nitrate ($C_{\text{pNO}_3, \text{tot}}$) generated from Tofware v3.3 ($s_{\overline{C}_{\text{pNO}_3, \text{tot}}}$), using Eqs. S14 and S15. The uncertainty of f_{pAmN} can be

assumed to be equal to that of f_{pON} due to their relationship ($f_{\text{pON}} + f_{\text{pAmN}} = 1$).

$$s_{\bar{C}_{\text{pON}}} = C_{\text{pNO}_3,\text{tot}} \cdot f_{\text{pON}} \cdot \sqrt{\left(\frac{s_{\bar{C}_{\text{pNO}_3,\text{tot}}}}{C_{\text{pNO}_3,\text{tot}}}\right)^2 + \left(\frac{s_{\bar{f}_{\text{pON}}}}{f_{\text{pON}}}\right)^2} \quad (\text{S14})$$

$$110 \quad s_{\bar{C}_{\text{pAmN}}} = C_{\text{pNO}_3,\text{tot}} \cdot f_{\text{pAmN}} \cdot \sqrt{\left(\frac{s_{\bar{C}_{\text{pNO}_3,\text{tot}}}}{C_{\text{pNO}_3,\text{tot}}}\right)^2 + \left(\frac{s_{\bar{f}_{\text{pAmN}}}}{f_{\text{pAmN}}}\right)^2}. \quad (\text{S15})$$

Note that the reported uncertainties are related to precision uncertainty only. Additional uncertainties associated with C_{pNO_3} concentration quantification (e.g. ionization efficiency, flow rate correction) are not included here to highlight values and trends in the apportionment. These uncertainties were estimated to be $\pm 34\%$ for 2σ using an SV-AMS by Bahreini et al. (2009). We might expect the uncertainty to be even smaller when using a CV inlet due reduced uncertainties from collection efficiency effects.

115

References

- Allan, J. D., Delia, A. E., Coe, H., Bower, K. N., Alfarra, M., Jimenez, J. L., Middlebrook, A. M., Drewnick, F., Onasch, T. B., Canagaratna, M. R., Jayne, J. T., and Worsnop, D. R.: A generalised method for the extraction of chemically resolved mass spectra from Aerodyne aerosol mass spectrometer data, *Journal of Aerosol Science*, 35, 909–922, <https://doi.org/10.1016/j.jaerosci.2004.02.007>, 2004.
- 120 Bahreini, R., Ervens, B., Middlebrook, A. M., Warneke, C., De Gouw, J. A., DeCarlo, P. F., Jimenez, J. L., Brock, C. A., Neuman, J. A., Ryerson, T. B., Stark, H., Atlas, E., Brioude, J., Fried, A., Holloway, J. S., Peischl, J., Richter, D., Walega, J., Weibring, P., Wollny, A. G., and Fehsenfeld, F. C.: Organic aerosol formation in urban and industrial plumes near Houston and Dallas, Texas, *Journal of Geophysical Research: Atmospheres*, 114, 2008JD011493, <https://doi.org/10.1029/2008JD011493>, 2009.
- 125 Carlton, A. G., De Gouw, J., Jimenez, J. L., Ambrose, J. L., Attwood, A. R., Brown, S., Baker, K. R., Brock, C., Cohen, R. C., Edgerton, S., Farkas, C. M., Farmer, D., Goldstein, A. H., Gratz, L., Guenther, A., Hunt, S., Jaeglé, L., Jaffe, D. A., Mak, J., McClure, C., Nenes, A., Nguyen, T. K., Pierce, J. R., De Sa, S., Selin, N. E., Shah, V., Shaw, S., Shepson, P. B., Song, S., Stutz, J., Surratt, J. D., Turpin, B. J., Warneke, C., Washenfelder, R. A., Wennberg, P. O., and Zhou, X.: Synthesis of the Southeast Atmosphere Studies: Investigating Fundamental Atmospheric Chemistry Questions, *Bulletin of the American Meteorological Society*, 99, 547–567, <https://doi.org/10.1175/BAMS-D-16-0048.1>, 2018.
- 130 Farmer, D. K., Matsunaga, A., Docherty, K. S., Surratt, J. D., Seinfeld, J. H., Ziemann, P. J., and Jimenez, J. L.: Response of an aerosol mass spectrometer to organonitrates and organosulfates and implications for atmospheric chemistry, *Proceedings of the National Academy of Sciences*, 107, 6670–6675, <https://doi.org/10.1073/pnas.0912340107>, 2010.
- Fry, J. L., Brown, S. S., Middlebrook, A. M., Edwards, P. M., Campuzano-Jost, P., Day, D. A., Jimenez, J. L., Allen, H. M., Ryerson, T. B., Pollack, I., Graus, M., Warneke, C., de Gouw, J. A., Brock, C. A., Gilman, J., Lerner, B. M., Dubé, W. P., Liao, J., and Welti, A.: Secondary organic aerosol (SOA) yields from NO₃ radical + isoprene based on nighttime aircraft power plant plume transects, *Atmospheric Chemistry and Physics*, 18, 11 663–11 682, <https://doi.org/10.5194/acp-18-11663-2018>, 2018.
- 135 Hu, W., Campuzano-Jost, P., Day, D. A., Croteau, P., Canagaratna, M. R., Jayne, J. T., Worsnop, D. R., and Jimenez, J. L.: Evaluation of the new capture vaporizer for aerosol mass spectrometers (AMS) through field studies of inorganic species, *Aerosol Science and Technology*, 51, 735–754, <https://doi.org/10.1080/02786826.2017.1296104>, 2017.
- 140 Hu, W., Day, D. A., Campuzano-Jost, P., Nault, B. A., Park, T., Lee, T., Croteau, P., Canagaratna, M. R., Jayne, J. T., Worsnop, D. R., and Jimenez, J. L.: Evaluation of the new capture vaporizer for aerosol mass spectrometers: Characterization of organic aerosol mass spectra, *Aerosol Science and Technology*, 52, 725–739, <https://doi.org/10.1080/02786826.2018.1454584>, 2018a.
- Hu, W., Day, D. A., Campuzano-Jost, P., Nault, B. A., Park, T., Lee, T., Croteau, P., Canagaratna, M. R., Jayne, J. T., Worsnop, D. R., and Jimenez, J. L.: Evaluation of the New Capture Vaporizer for Aerosol Mass Spectrometers (AMS): Elemental Composition and Source Apportionment of Organic Aerosols (OA), *ACS Earth and Space Chemistry*, 2, 410–421, <https://doi.org/10.1021/acsearthspacechem.8b00002>, 2018b.
- 145 Takeuchi, M. and Ng, N. L.: Chemical composition and hydrolysis of organic nitrate aerosol formed from hydroxyl and nitrate radical oxidation of α -pinene and β -pinene, *Atmospheric Chemistry and Physics*, 19, 12 749–12 766, <https://doi.org/10.5194/acp-19-12749-2019>, 2019.